



Dual HDAC–BRD4 inhibitors endowed with antitumor and antihyperalgesic activity

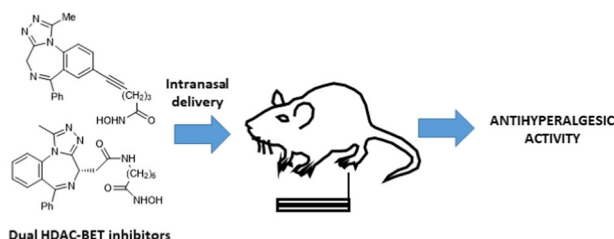
Soumia Maach¹ · Niccolò Chiaramonte¹ · Vittoria Borgonetti¹ · Federica Sarno² · Federica Pierucci³ · Silvia Dei¹ · Elisabetta Teodori¹ · Lucia Altucci^{2,4} · Elisabetta Meacci³ · Nicoletta Galeotti¹ · Maria Novella Romanelli¹

Received: 28 January 2022 / Accepted: 16 April 2022
© The Author(s) 2022

Abstract

Histone deacetylases (HDAC) are enzymes that regulate the concentration of acetylated histones which, in turns, interact with the bromodomain (BRD) of BET (Bromodomain and Extracellular domain) proteins to affect transcriptional activity. Simultaneous blockade of both epigenetic players has shown synergistic effects in a variety of cancer cell lines. In this paper we report the design, synthesis and activity of new dual inhibitors, obtained by adding a methyltriazole moiety to some HDAC inhibitors carrying a benzodiazepine core, which were previously developed by us. An Alphascreen FRET assay showed that the compounds were able to interact with BRD4-1 and BRD4-2 proteins, with some selectivity for the latter, while the HDAC inhibiting properties were measured by means of an immunoprecipitation assay. The antiproliferative activity was tested on C26 adenocarcinoma, SSMC2 melanoma and SHSY5Y neuroblastoma cells. Interestingly, both compounds were endowed with antihyperalgesic activity in the mouse Spared Nerve Injury (SNI) model.

Graphical abstract



Keywords Dual inhibitors · BRD4 inhibitors · HDAC inhibitors · Antiproliferative activity · Antihyperalgesic activity · Spared Nerve Injury model

Supplementary information The online version contains supplementary material available at <https://doi.org/10.1007/s00044-022-02896-w>.

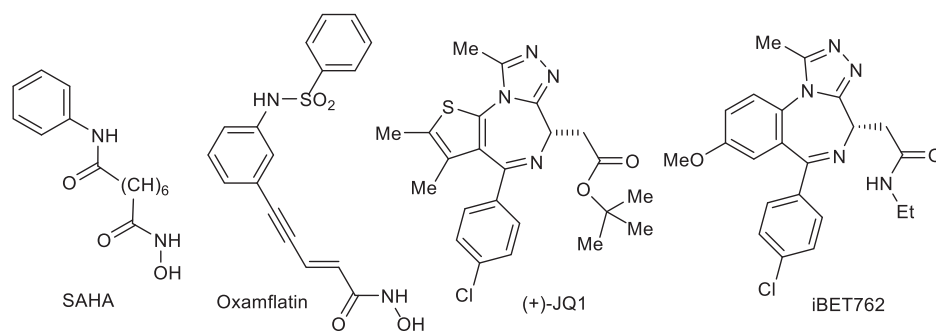
✉ Maria Novella Romanelli
novella.romanelli@unifi.it

- ¹ Department of Neurosciences, Psychology, Drug Research and Child Health (NeuroFarBa), University of Florence, Florence, Italy
- ² Department of Precision Medicine, University of Campania ‘Luigi Vanvitelli’, Napoli, Italy
- ³ Department of Experimental and Clinical Biomedical Sciences ‘Mario Serio’, University of Florence, Florence, Italy
- ⁴ BIOGEM, Molecular Biology and Genetics Research Institute, Ariano Irpino, AV, Italy

Introduction

Epigenetics is defined as the study of the mechanisms involved in the regulation of gene expression without altering gene sequence [1]. The epigenetic code results from the combined activity of different players, which write, erase and read the structural modifications that affect chromatin structure and regulate gene expression. Histone deacetylase (HDAC) are among the best characterized “erasers”. This family of enzymes removes the acetyl groups from the histone lysine residues, contributing to chromatin compaction and thus to gene silencing. HDAC are divided into four different classes: class I, II, and IV comprise 11 different Zn²⁺-dependent isoforms, while in

Fig. 1 Structure of selected HDACi and BRD4 inhibitors



class III (sirtuins) seven NAD-dependent isoforms are described [2]. Five HDAC inhibitors (HDACi) have been approved for hematological malignancies, but several others are presently in clinical trials for different kinds of tumors [3]. The pan inhibitor SAHA (Suberoylanilide hydroxamic acid, Fig. 1) is the first HDACi approved for therapy.

The structure of HDACi can be generally divided into three different components: a Zn^{2+} -binding group, a linker, and a cap. The most frequent Zn^{2+} -binding group is the hydroxamate moiety, as in SAHA; by chelating the metal ion it blocks the enzymatic activity. The cap, which occupies the entrance to the active site, is often an aromatic group of various size. The linker, which connects the other two components, is a hydrophobic group of variable length and composition [4].

Bromodomain and extra-terminal domain (BET) proteins are able to enhance transcriptional activity by reading acetylated histones through the bromodomain (BRD). BET proteins comprise four different isoforms, BRD2, BRD3, BRD4, and BRDT; each contains two tandem bromodomains (BD1) and (BD2) [5]. BRD4 is the most investigated member of the BET family; iBET762 and JQ1 (Fig. 1) are examples of BRD4-selective inhibitors carrying a triazolodiazepine structure. The important role of BRD4 in key transcriptional pathways made this protein an attracting target for the development of anticancer agents [3, 6].

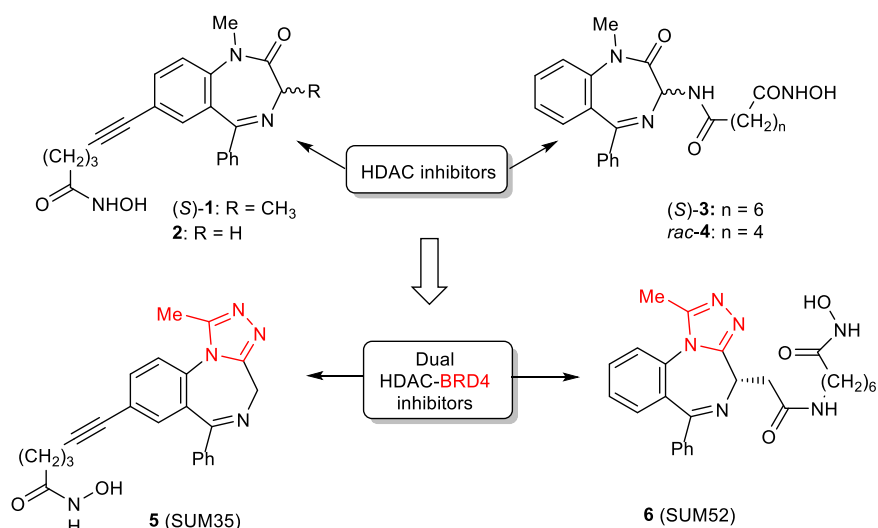
Several lines of evidence, mainly coming from studies on hematological malignancies, have shown that the inhibition of HDAC and BET proteins regulates the transcription of common genes, such as, for instance, *Myc* and *Bcl2*. Indeed, the co-administration of HDACi and BET inhibitors has shown synergistic effects in hematological and solid tumors (reviewed in [7]). On these bases, by applying the strategy of polypharmacology, several compounds carrying both pharmacophores for the simultaneous inhibition of HDAC and BET proteins have been prepared and tested in a variety of cancer cell lines (reviewed in ref. [3, 8, 9]).

While the clinical use of HDACi and BRD4 inhibitors as antitumor agents is well established, in recent years these targets have been proposed also for the development of drugs for other therapeutic applications, such as neurodegenerative, neurological, cardiovascular, inflammation and

immune disorders [2, 10–13]. In particular, several evidences support the role of epigenetic mechanisms in the development of conditions such as neuropathic or chronic pain, in which hyperalgesia can result from changes in the expression of pain-related receptors or ion channels, leading to cellular and tissue adaptation [14]. The ability of HDACi to relieve chronic pain is already established (reviewed in [15]), and evidence of the involvement of BRD4 in nociception has also been reported [16–19]. Some of our research group have recently shown that the synergistic effect of HDACi and BRD4 inhibitors is maintained in animal models of neuropathic pain. Indeed, the co-administration of SAHA and iBET762 was proven to be significantly more effective than the single agents on allodynia induced by spared nerve injury (SNI) in mice [20]. Since the anticancer chemotherapy is often associated to the development of peripheral neuropathies [21, 22], we speculated that the simultaneous blockade of HDAC and BRD4 proteins could be further advantageous, because it could combine the anticancer activity with a relief of chemotherapy-induced neuropathic pain.

As a step forward, we designed dual HDAC–BRD4 inhibitors as multitarget ligands, to be tested as anticancer and in animal models of neuropathic pain. Our design started from a series of HDACi, hydroxamates previously described by our group (compounds 1–4, Fig. 2), carrying a saturated or unsaturated chain as linker (as in SAHA and oxamflatin, Fig. 1), and a 5-phenyl-1,4-benzodiazepin-2-one moiety as cap; the hydroxamate-linker moiety was attached to different positions of the benzodiazepine core. These compounds showed IC_{50} values in the micromolar range for HDAC inhibition and interesting anticancer activity in different tumor cell lines [23–27]. Later, it was found that *rac-4* displayed antihyperalgesic activity in a mouse model of neuropathic pain [28]. Since it is reported in the literature that the addition of a methyltriazole moiety to the benzodiazepine core could introduce some affinity for the BRD domain [29], we did the same modification on our molecules. Therefore, we designed and prepared compounds 5 and 6 (Fig. 2) which contain both the HDACi pharmacophore (the Zn-chelating hydroxamate moiety at the end of a long chain, as in SAHA and oxamflatin) and the 1-methyl-6-phenyl-4H-benzo[f][1,2,4]triazolo

Fig. 2 HDACi lead compounds and designed HDAC–BRD4 dual inhibitors



[4,3-*a*][1,4]diazepine moiety typical of BRD4 inhibitors such as iBET762. In compound **6**, the NHCO group present in **3** and **4** has been replaced by an acetamide moiety, as in iBET761, since this modification has been reported to improve the properties of BRD inhibitors [30]. Both enantiomers of compound **3** were active as HDAC inhibitors, but with low eudismic ratios in the *in vitro* tests [26]. Thus, we decided to prepare only *S*-**6**, because it is known that the *R* enantiomers of JQ1 and iBET762 are devoid of affinity for BRD4 [30, 31].

The new compounds were tested for their ability to inhibit HDAC and BRD4, to reduce the growth of cancer cells and to increase pain threshold in the mouse SNI model. While this work was in progress, compounds with structure similar to **6**, deriving from hybridization of SAHA and JQ1, were reported in the literature and tested as anti-tumor agents [32].

Results and discussion

Synthesis of compounds 5 and 6

Compound **5** was prepared as reported in Scheme 1. The reaction of 7-iodo-5-phenyl-1,3-dihydro-2H-benzo[*e*][1,4]diazepin-2-one [23] with Lawesson reagent gave **7**, which was treated with hydrazine obtaining **8**. The triazole ring closure was accomplished using ethyl orthoacetate; **9** was obtained in 41% yields. A Sonogashira reaction between **9** and *N*-[(tetrahydro-2H-pyran-2-yl)oxy]hex-5-ynamide **10**, prepared from 5-hexynoic acid and *O*-(tetrahydro-2H-pyran-2-yl)hydroxylamine (Scheme 1B), afforded **11**. The protecting group was removed using HCl in dioxane, obtaining **5** (SUM35) in 37% yields.

The synthetic pathway for the synthesis of **6** is reported in Scheme 2. Methyl (*S*)-2-(2-oxo-5-phenyl-2,3-dihydro-

1H-benzo[*e*][1,4]diazepin-3-yl)acetate **13** was prepared using the usual sequence for the synthesis of the benzo-diazepine ring [26]: 2-aminobenzophenone was first reacted with methyl (*S*)-3-(((9H-fluoren-9-yl)methoxy)carbonyl)amino)-4-chloro-4-oxobutanoate [33], and the intermediate amide **12** was deprotected under basic conditions and cyclized to **13** using acetic acid. The reaction with P₄S₁₀ gave **14**, which was treated with hydrazine obtaining **15**. This compound was treated first with acetyl chloride and then with acetic acid yielding methyl (*S*)-2-(1-methyl-6-phenyl-4H-benzo[*f*][1,2,4]triazolo[4,3-*a*][1,4]diazepin-4-yl)acetate **16**. Basic hydrolysis gave the carboxylic acid **17** which was reacted with methyl 7-aminoheptanoate using HATU as coupling reagent to give **18**. Final treatment with hydroxylamine under basic conditions gave the desired product **6** (SUM52).

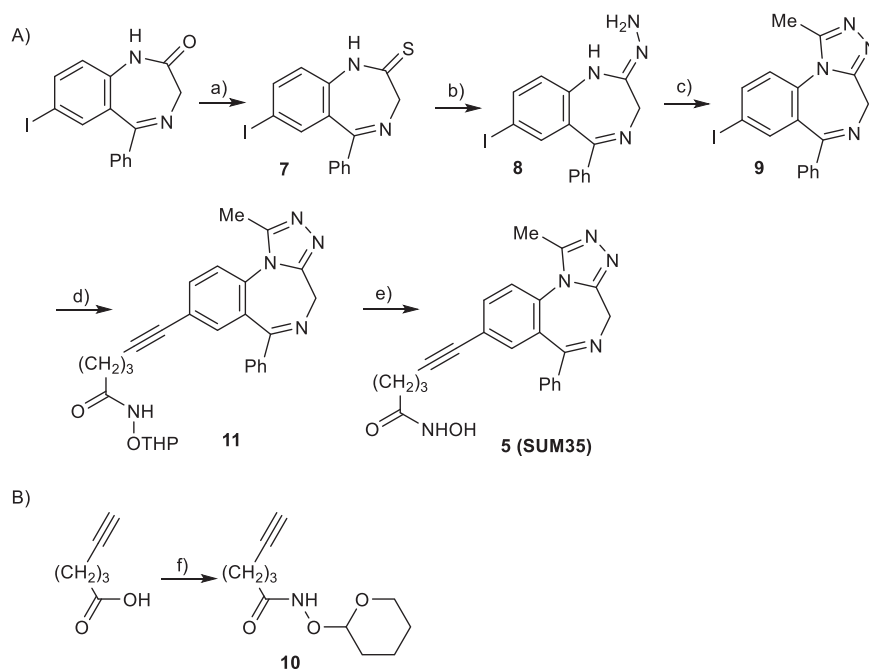
Properties of compounds 5 and 6

The Swiss-ADME (<http://www.swissadme.ch/>) tool was used to predict the physicochemical properties and the pharmacokinetic parameters of compounds **5** and **6**. The result are reported in Table S1 (Supplementary Information). Both compounds are predicted to have high gastrointestinal absorption, but to be unable to cross the Blood Brain Barrier. In order to avoid permeability problems, we decided to use an intranasal route of administration. The potential to inhibit the major human CYP isoforms was anticipated to be high for **6** but not for **5**.

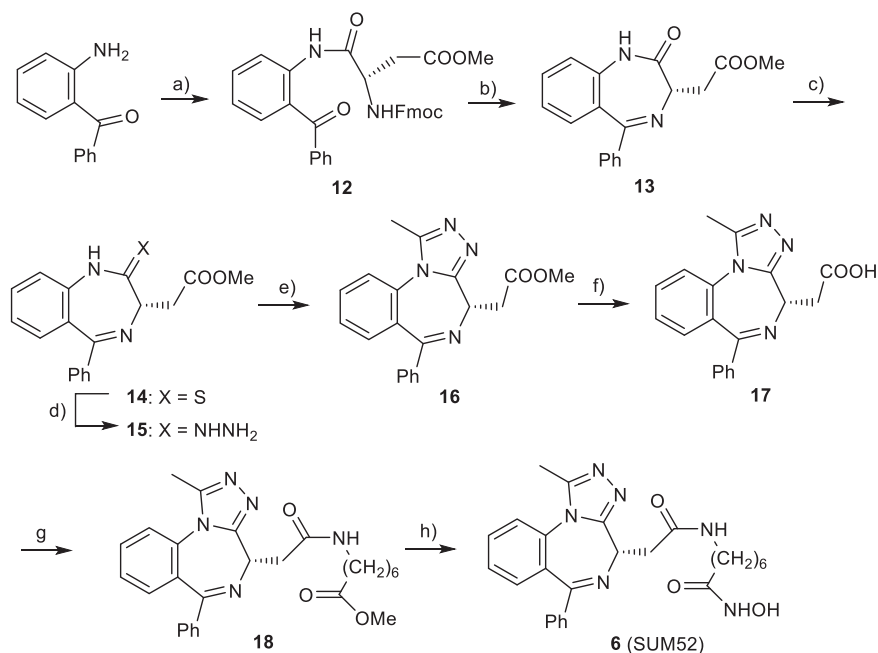
Interaction with BRD4 and HDAC proteins

The ability of compounds **5** and **6** to bind to BRD4-BD1 and BRD4-BD2 was tested by Reaction Biology using an Alphascreen FRET assay in comparison with (+)-JQ1 (Fig. 3). Compounds **5** and **6** were both able to inhibit the

Scheme 1 Synthetic route to compounds **5** (A) and **10** (B). Reagents and conditions: (a) Lawesson reagent, toluene, reflux; (b) $\text{H}_2\text{N-NH}_2$, THF; (c) triethyl orthoacetate, EtOAc, *p*-toluenesulfonic acid, reflux; (d) *N*-((tetrahydro-2H-pyran-2-yl)oxy)hex-5-ynamide **10**, Pd(PPh_3)₄, CuI, Et₃N, 55 °C; (e) HCl 4 N, dioxane; (f) *O*-tetrahydropyranyl-hydroxylamine, EDC, DMAP, CHCl_3



Scheme 2 Synthetic route to compound **6**. Reagents and conditions: (a) (S) Fmoc-NHCH(COCl)CH₂COOMe, CHCl_3 , 60 °C; (b) (i) piperidine, THF; (ii) AcOH, THF; (c) P_4S_{10} , Na_2CO_3 , 1,2-dichloroethane; (d) $\text{H}_2\text{N-NH}_2$, THF, 5 °C; (e) (i) CH_3COCl , THF, 0 °C, (ii) AcOH, reflux; (f) NaOH 1 M, THF/MeOH; (g) $\text{H}_2\text{N-(CH}_2)_6\text{-COOMe}$, HATU, Et₃N, DMF, RT; (h) NH_2OH , KOH, MeOH

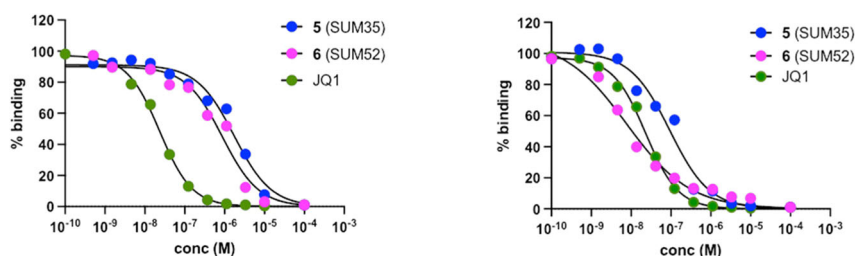


binding of the acetylated histone peptide, with different potency, as **5** turned to be less potent than **6** on both bromodomains. On BRD4-BD1 compound **5** showed a half-maximum inhibitory concentration (IC_{50}) value in the low micromolar range ($\text{IC}_{50} = 1.722 \mu\text{M}$) while **6** was about twice more potent ($\text{IC}_{50} = 0.758 \mu\text{M}$). On BRD4-BD2 both compounds displayed higher potency, with **6** showing an IC_{50} value one order of magnitude lower than **5** ($\text{IC}_{50} = 10.5$ and 118 nM , respectively). Therefore,

both **5** and **6** displayed a preference for BRD4-BD2, being, respectively, 14 and 72 times more active on this bromodomain than on BRD4-BD1. The IC_{50} values for (+)-JQ1, taken as reference, are in the same range with respect to the literature values [31].

A fluorometric assay was first used to measure the ability of compounds **5** and **6** to inhibit HDAC activity; however, the intrinsic fluorescence of compound **6** precluded the determination of the IC_{50} value. So, both compounds were tested at

Fig. 3 Inhibition curves on BRD4-1 (left) and BRD4-2 (right) for **5** (SUM35, blue) and **6** (SUM52, red) in comparison with (+)-JQ1 (green)



	6 (SUM52)	5 (SUM35)	JQ1
Hill slope	-0.86	-0.92	-1.06
IC ₅₀ (μM)	0.76	1.72	0.023

	6 (SUM52)	5 (SUM35)	JQ1
Hill slope	-0.67	-1.02	-0.95
IC ₅₀ (nM)	10.50	118.50	12.58

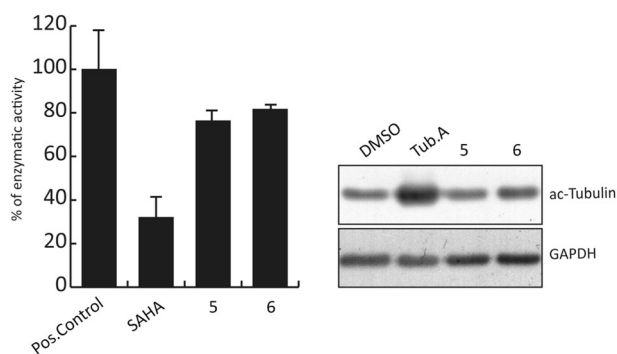


Fig. 4 Inhibitory activity of compounds **5** and **6** on HDAC. Left: activity determined on HDAC1 using an immunoprecipitation assay. SAHA (5 μM) was used as a control. Right: effect of **5** (SUM35) and **6** (SUM52) on tubulin acetylation, in comparison with Tubastatin A (Tub.A) (10 μM). GAPDH was used for protein normalization

10 μM using an immunoprecipitation assay, but only 20% of HDAC activity inhibition was observed (Fig. 4, left). The results were also confirmed measuring the tubulin acetylation levels (Fig. 4, right).

Antitumor activity

The antitumor activity of compounds **5** and **6** was evaluated in vitro, using two cell lines, C26 adenocarcinoma cells and SSM2C melanoma cells. The treatment with the BET/HDAC dual inhibitors caused a dose- and time-dependent reduction of cell proliferation. In fact, as shown in Fig. 5A, the concentrations of 40 and 60 μM were able to significantly reduce cell proliferation at 24 h, whereas both compounds were ineffective at 20 μM. Although the antitumor effect was observed using both BET/HDAC dual inhibitors, the two cell lines showed different sensibility to the compounds. In fact, the antitumor effect reached the maximum of 90% when SSM2C cells were incubated with compound **6** for 24 h (Fig. 5A, left), whereas in the same experimental conditions, this compound determined a

decrease of approximately 55% in the proliferation of C26 adenocarcinoma cells (Fig. 5A, right). In both cell lines, compound **5** was less effective. Notably, both compounds were less effective after long term incubation (48 h) either when administered to SSM2C cells than C26 adenocarcinoma cells (Fig. 5B), indicating a progressive loss of stability/effectiveness of the molecule in the cell medium.

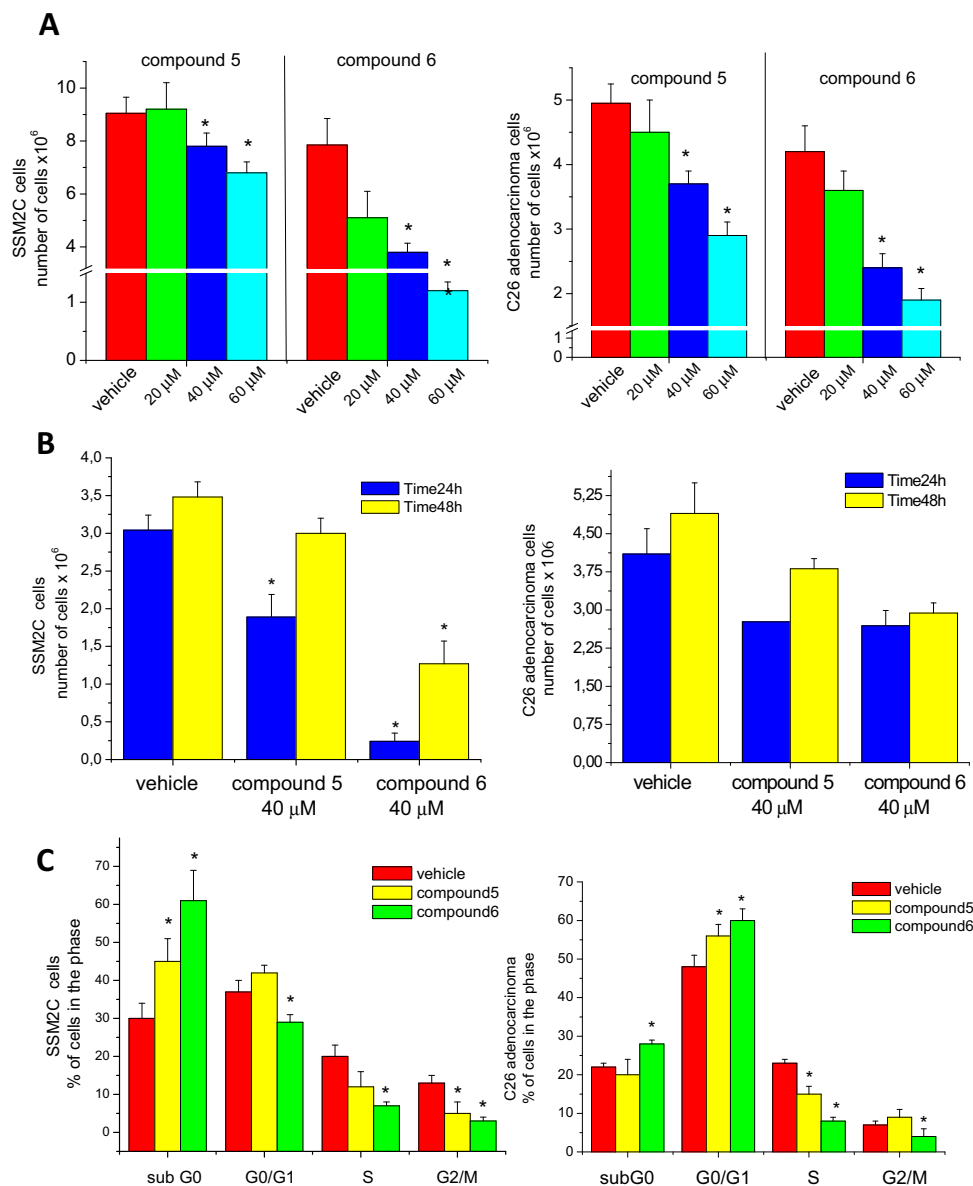
To investigate the cellular effects of the compounds **5** and **6** in more detail, cell cycle was analyzed by TALI cytometer. As reported in Fig. 5C, the treatment of SSM2C cells with compound **5** (60 μM) or compound **6** (60 μM) led to accumulation of cells in the subG0 phase paralleled by a decrease of S phase and stronger reduction of G2/M-phase fraction, indicating cell cycle inhibition and cell death. On the contrary, the number of subG1/G0 phase cells was significantly lower after treatment of C26 adenocarcinoma cells with compound **5** or compound **6**, paralleled by a reduction of S phase (Fig. 5C). Compound **6**, but not compound **5**, significantly negatively affects G2/M-phase cell fraction.

The effect of the BET/HDAC dual inhibitors **5** and **6** was evaluated also on the neuroblastoma cell line SHSY5Y. As shown in Fig. 6 and in Fig. S1 (Supplementary Information), similarly to the known inhibitor iBET762 (0.75 μM), either compounds **5** (30 μM) and compound **6** (15 μM) alone were able to reduce cell proliferation (~50%) (Fig. 6, left). Notably, when SH-SY5Y cells were incubated with iBET combined with compound **5** or compound **6** the antiproliferative action of iBET was significantly decreased. The increase in the expression level of the marker of cell cycle arrest, the Cyclin-dependent Kinase Inhibitor p21, observed either in cells treated with iBET and compound **6** alone, was also significantly decreased when the cells were incubated with the two inhibitors together (Fig. 6, right). It seems that boosting the interaction with BRD4 proteins does not translate into an improvement in the antiproliferative activity, suggesting that a balanced inhibition of both targets is crucial for an optimal effect.

Fig. 5 A Effect of compounds **5** and **6** on proliferation of SSM2C cells (left) and C26 cells (right) after 24 h incubation.

B Comparison of the effect of compounds **5** and **6** on proliferation of SSM2C cells (left) and C26 cells (right) after 24 h and 48 h incubation.

C Effect of compounds **5** and **6** on cell cycle on SSM2C cells (left) and C26 cells (right) measured by means of TALI cytometer, after 24 h incubation. * $p < 0.05$ vs. controls



Antihyperalgesic activity

The antihyperalgesic activity of **5** and **6** was investigated by using the SNI model in mice. This model allows to establish a persistent and significant mechanical and thermal allodynia in the ipsilateral side (i; injured hind limb) of SNI mice, compared to the contralateral side (c; uninjured hind limb), starting from 3 days after surgery up to 28 days [34]. Seven days post-SNI surgery, the dose–response curve for compounds **5** and **6** has been performed on thermal and mechanical allodynia (Table 1) using Hargreave's plantar test and von Frey filaments, respectively. Both molecules have been administered 60 min before testing, according to the results obtained in time course experiment. In the plantar test, compound **6** showed

antihyperalgesic effects starting from the dose of 50 μM, with a significant peak at the dose of 75 μM, while compound **5** reversed the allodynia at higher doses (75 and 100 μM) in the ipsilateral side (Table 1). Similarly, in the von Frey measurements, compounds **5** and **6** showed a peak of effect at the dose of 100 and 75 μM, respectively (Table 1). Both molecules lost their activity at higher concentrations, highlighting a bell-shape curve.

A comparison of the antihyperalgesic activity of compounds **5** and **6** against thermal and mechanical allodynia is reported in Fig. 6. Compound **6** reduced the mechanical allodynia with an efficacy ~1.5-fold higher than compound **5** (Fig. 7b). This effect was not observed in the thermal allodynia test, in which both molecules showed a similar efficacy profile (Fig. 7a).

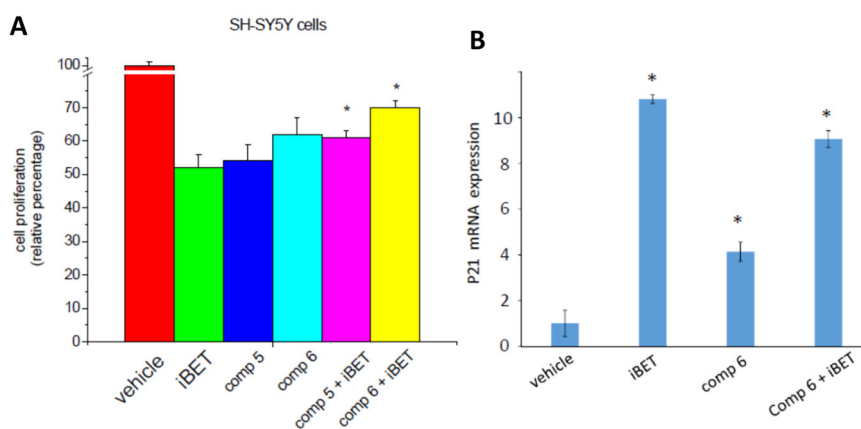


Fig. 6 **A** Cell proliferation analysis. Cell counting of SHSY5Y neuroblastoma cell line (left) treated for 24 h in absence (vehicle) and/or in presence of inhibitor iBET762 (0.75 μ M), either compounds **5** (30 μ M) and compound **6** (15 μ M). Data were means \pm SEM of at least three independent experiments performed in quadruplicate and were reported in the graph as percentage relative to untreated cells (vehicle) set as 100. One-way ANOVA test, **P* < 0.05 vs. vehicle. **B** Expression levels of the Cyclin-dependent Kinase Inhibitor p21 by Real-Time PCR (right). Total RNA was obtained from SHSY5Y neuroblastoma

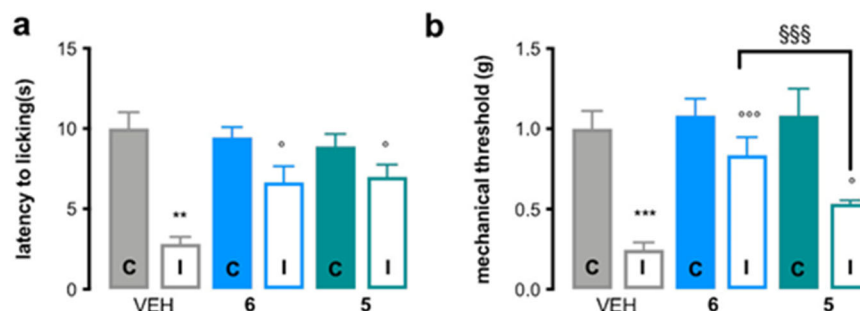
cell line treated for 24 h in absence (vehicle) and/or in presence of inhibitor iBET762, either compounds **6**. Total RNA was purified and reverse transcribed as in Methods. Real-Time PCR was performed using specific forward and reverse primers for P21. Data were presented as fold change (mean \pm SEM) of at least three independent experiments and were reported in the table as percentage relative to untreated cells (vehicle). One-way ANOVA test, **P* < 0.05; ***P* < 0.01 vs. vehicle; ^{\$}*P* < 0.05 vs. compound **6**

Table 1 Dose–response curve for thermal and mechanical antihyperalgesic activity of compound **6** (SUM52) and compound **5** (SUM35) in the SNI model

Treatment	Doses (μ M)	Thermal threshold (s)		Mechanical threshold (g)	
		Contra	Ipsi	Contra	Ipsi
Vehicle		10.52 \pm 2.99	1.69 \pm 0.58**	0.86 \pm 0.19	0.20 \pm 0.05**
6 (SUM52)	10	11.56 \pm 3.17	1.76 \pm 0.69**	0.86 \pm 0.26	0.21 \pm 0.07**
6 (SUM52)	50	10.63 \pm 1.67	6.73 \pm 1.01	0.89 \pm 0.13	0.67 \pm 0.09**
6 (SUM52)	75	10.80 \pm 1.76	7.10 \pm 0.72	0.85 \pm 0.15	0.55 \pm 0.10
6 (SUM52)	100	10.73 \pm 2.77	3.30 \pm 0.30*	0.89 \pm 0.27	0.34 \pm 0.09*
5 (SUM35)	10	8.33 \pm 0.73	2.76 \pm 0.85**	0.87 \pm 0.26	0.17 \pm 0.01**
5 (SUM35)	50	9.36 \pm 1.72	2.80 \pm 0.43**	0.80 \pm 0.13	0.21 \pm 0.09*
5 (SUM35)	75	8.93 \pm 1.64	5.13 \pm 0.71	0.98 \pm 0.14	0.29 \pm 0.11*
5 (SUM35)	100	8.66 \pm 1.45	7.06 \pm 0.77	0.87 \pm 0.20	0.60 \pm 0.20
5 (SUM35)	200	9.16 \pm 0.99	4.13 \pm 0.23*	0.89 \pm 0.13	0.32 \pm 0.08*

p* < 0.05; *p* < 0.01 vs. contra (one-way ANOVA)

Fig. 7 Comparison of efficacy between compound **6** (SUM52; 50 μ M) and compound **5** (SUM35; 100 μ M) for the thermal (a) and mechanical (b) allodynia (***p* < 0.001; ***p* < 0.01 vs. VEH contra; °°°*p* < 0.001 vs. VEH ipsi; two-way ANOVA)



Conclusions

In conclusion, we have synthesized and tested two dual inhibitors (compounds **5** and **6**), showing different interaction with

BRD4 bromodomains. Compound **6** was 2 and 11 times more potent than **5** on BRD4-BD1 and BRD4-BD2, respectively. Moreover, both molecules showed higher affinity on BRD4-BD2 (14 and 72 times, respectively) than on BRD4-BD1.

The compounds were able to inhibit nuclear HDAC only with high IC_{50} values ($>10 \mu\text{M}$), while they were inactive toward HDAC6. Their antiproliferative activity has been tested on C26 adenocarcinoma and SSMC2 melanoma cell lines, on which the compounds showed a significant activity at 40 and 60 μM concentration. On the neuroblastoma cell line SHSY5Y compounds **5** and **6** reduced cell viability at, respectively, 30 and 15 μM . The concentration of the Cyclin-dependent Kinase Inhibitor p21 was increased after treatment with compound **6**. Co-administration of iBET762 with either compound **5** or **6** reduced the antiproliferative effect, suggesting that the activity on both targets should be balanced to obtain an optimal effect. Both compounds were endowed with antihyperalgesic activity when tested on thermal and mechanical allodynia in the mouse SNI model, suggesting that dual HDAC/BRD4 inhibitors can be effective to ameliorate neuropathic pain. This property makes dual HDAC/BRD4 inhibitors promising adjuvant to anticancer therapies in which painful neuropathies represent a prominent side effect. Work is underway to improve the inhibitory profile of compounds **5** and **6** and to test them in models of chemotherapy-induced neuropathies.

Experimental

Chemistry

All melting points were taken on a Büchi apparatus and are uncorrected. NMR spectra were recorded on a Bruker Avance 400 spectrometer (400 MHz for ^1H NMR, 100 MHz for ^{13}C). Chromatographic separations were performed on a silica gel column by gravity chromatography (Kieselgel 40, 0.063–0.200 mm; Merck) or flash chromatography (Kieselgel 40, 0.040–0.063 mm; Merck). Yields are given after purification, unless differently stated. When reactions were performed under anhydrous conditions, the mixtures were maintained under nitrogen.

ESI-MS spectra were obtained using a Varian 1200L triple quadrupole system (Palo Alto, CA, USA) equipped by Elektrospray Source (ESI). High resolution mass spectrometry analyses were performed with a Thermo Finnigan LTQ Orbitrap mass spectrometer equipped with an electrospray ionization source (ESI). Analysis were carried out in positive ion mode monitoring protonated molecules, $[\text{M} + \text{H}]^+$ species, and it was used a proper dwell time acquisition to achieve 60,000 units of resolution at Full Width at Half Maximum. Elemental composition of compounds was calculated on the basis of their measured accurate masses, accepting only results with an attribution error <5 ppm and a not integer RDB (double bond/ring equivalents) value, in order to consider only the protonated species [35]. Compounds were named following IUPAC rules.

7-iodo-5-phenyl-1,3-dihydro-2H-benzo[e][1,4]diazepine-2-thione **7**

7-Iodo-5-phenyl-1,3-dihydro-2H-benzo[e][1,4]diazepin-2-one [23] (0.3 g, 0.83 mmol) and Lawesson reagent (0.2 g, 0.50 mmol) were heated in toluene (10 mL) under reflux for 3 h, monitoring the reaction by TLC (hexane-ethyl acetate 1:1). After removal of the solvent under vacuum, the residue was purified by flash chromatography, yielding **7** with 92 % yield. ^1H -NMR (DMSO- d_6) (δ): 4.52 (bs, 2H, $\text{CH}_2\text{C}=\text{S}$); 7.11 (d, $J = 8.8$ Hz, 1H, H-8 or H-9); 7.35–7.53 (m, 6H, Ph + H-6); 7.89 (d, $J = 8.8$ Hz, 1H, H-9 or H-8); 12.72 (bs, 1H, NH) ppm.

8-iodo-1-methyl-6-phenyl-4H-benzo[f][1,2,4]triazolo[4,3-a][1,4]diazepine **9**

Compound **7** was solubilized in THF (10 mL) and treated with 0.3 mL of hydrazine hydrate at room T until disappearance of the starting material (TLC, $\text{CH}_2\text{Cl}_2/\text{MeOH}/\text{NH}_3$ 93:7:03). The residue was treated with CH_2Cl_2 and H_2O ; a solid precipitated which was collected, washed with diethyl ether and dried, obtaining 0.21 g of 2-hydrazono-7-iodo-5-phenyl-2,3-dihydro-1H-benzo[e][1,4]diazepine **8**, which was used as such in the following step: it was dissolved in ethyl acetate (10 mL), treated with triethyl orthoacetate (0.6 mL, 6 eq) and a catalytic amount of *p*-toluenesulfonic acid, the mixture was heated under reflux until disappearance of the starting material (about 30'; TLC, $\text{CH}_2\text{Cl}_2/\text{MeOH}/\text{NH}_3$ 90:10:1). After cooling, the mixture was diluted with ethyl acetate; a solid precipitated which was purified by means of flash chromatography obtaining the desired compound **9** (0.17 g, 76% yield). ^1H -NMR (CDCl_3 , δ): 2.61 (s, 3H, CH_3); 4.08 (d, $J = 12.8$ Hz, 1H, *CHH*); 5.46 (d, $J = 12.8$ Hz, 1H, *CHH*); 7.17 (d, $J = 8.4$ Hz, 1H, H-10); 7.33–7.41 (m, 2H, ar); 7.41–7.47 (m, 1H, ar); 7.47–7.54 (m, 2H, ar); 7.75 (s, 1H, H-7); 7.96 (dd, $J = 8.4$, 2.0 Hz, 1H, H-9) ppm. ^{13}C -NMR (APT, CDCl_3 , δ): 12.31 (CH_3), 46.30 (CH_2), 91.92 (C-I), 124.81 (CH), 128.47 (CH), 129.31 (CH), 130.93 (CH), 133.41 (C), 138.58 (C), 140.48 (CH), 140.53 (CH), 150.06 (C), 155.05 (C), 167.76 (C) ppm. ESI-MS ($\text{C}_{17}\text{H}_{13}\text{IN}_4$) 401.0 ($\text{M} + \text{H}$) $^+$.

N-[(Tetrahydro-2H-pyran-2-yl)oxy]hex-5-ynamide **10**

Commercially available 5-hexynoic acid (0.5 g, 4.46 mmol) and O-(tetrahydropyranyl)-hydroxylamine (0.575 g, 1.1 eq) were dissolved in CHCl_3 , EDCI (1.13 g, 1.3 eq) and DMAP (0.055 g, 0.1 eq) were added and the mixture was left stirring overnight at room T. The mixture was then partitioned between H_2O and CHCl_3 , the organic solvent was collected, dried (Na_2SO_4) and the solvent was removed under vacuum affording a residue which was purified by means of flash chromatography. The title compound was obtained as an oil

in 95% yields. ¹H-NMR (CDCl₃, δ, mixture of conformers): 1.49–1.88 (m, 8H, 4CH₂); 1.94 (s, 1H, CH); 2.15–2.62 (m, 4H, CH₂CO + CH₂C≡); 3.55–3.62 (m, 1H, CHHO); 3.82–3.96 (m, 1H, CHHO); 4.75–4.93 (m, 1H, CHO); 8.45 (bs, 0.3H, NH); 8.64 (bs, 0.7H, NH) ppm. ¹³C-NMR (MeOD, δ): 17.15, 18.02, 24.27, 24.82, 27.54, 31.20, 61.60, 68.92, 82.57 (C≡), 101.74 (CHO), 170.55 (CO) ppm. ESI-MS (C₁₁H₁₇NO₃) 234.0 (M + Na)⁺.

6-(1-Methyl-6-phenyl-4H-benzof[1,2,4]triazolo[4,3-a][1,4]diazepin-8-yl)-N-((tetrahydro-2H-pyran-2-yl)oxy)hex-5-ynamide 11

A mixture of **9** (0.16 g, 0.4 mmol), **10** (0.13 g, 0.6 mmol), CuI (0.009 g, 0.05 mmol), Pd(Ph)₄ (0.0185 g, 0.16 mmol) in Et₃N (5 mL) was heated at 55 °C for 22 hr. After removal of solvent, the residue is partitioned between ethyl acetate and a saturated solution of NH₄Cl. Drying (Na₂SO₄) and removal of solvent gave a residue which was purified by flash chromatography, obtaining the title compound in 40% yield. ¹H-NMR (CDCl₃, δ): 1.47–1.82 (m, 6H); 1.91 (p, J = 7.2 Hz, 2H); 2.18–2.29 (m, 2H, CH₂CO); 2.45 (t, J = 7.2 Hz, 2H); 2.61 (s, 3H); 3.53–3.60 (m, 1H, CHHO); 3.82–3.92 (m, 1H, CHHO); 4.03 (d, J = 12.8 Hz, 1H); 4.90 (bs, 1H, CH); 5.46 (d, J = 12.8 Hz, 1H); 7.32–7.39 (m, 3H, ar); 7.41–7.46 (m, 2H, ar); 7.48–7.53 (m, 2H, ar); 7.63 (dd, J = 8.4, 1.6 Hz, 1H, ar); 8.31 (bs, 1H, NH) ppm. ¹³C-NMR (MeOD, δ): 12.35 (CH₃), 18.59 (CH₂), 18.87 (CH₂), 24.96 (CH₂), 27.99 (CH₂), 29.70 (CH₂), 30.32 (CH), 46.34 (CH₂), 62.62 (CH₂), 79.44 (C), 92.11 (C), 123.22 (CH), 123.39 (C), 128.38 (CH), 129.25 (C), 129.35 (CH), 130.75 (CH), 132.65 (C), 134.35 (CH), 134.75 (CH), 138.91 (C), 153.12 (C), 155.12 (C), 168.61 (C) ppm. ESI-MS (C₂₈H₂₉N₅O₃) 484.2 (M + H)⁺.

N-Hydroxy-6-(1-methyl-6-phenyl-4H-benzof[1,2,4]triazolo[4,3-a][1,4]diazepin-8-yl)hex-5-ynamide 5 (SUM35)

To a stirred solution of **11** (0.026 g) in dioxane (1 mL) HCl (2 N, 0.11 mL) was added and the mixture left stirring at room T for 1 h. The mixture was partitioned between CH₂Cl₂ and NaHCO₃ (saturated solution). Drying (Na₂SO₄) and removal of solvent gave a residue which was purified by flash chromatography (CH₂Cl₂/MeOH 8:2), obtaining the title compound in 43% yield. ¹H-NMR (MeOD, δ): 1.83 (p, J = 7.2 Hz, 2H); 2.19 (t, J = 7.2 Hz, 2H); 2.42 (t, J = 7.2 Hz, 2H); 2.63 (s, 3H); 4.18 (d, J = 13.2 Hz, 1H); 5.22 (d, J = 13.2 Hz, 1H); 7.32 (s, 1H, ar); 7.33–7.38 (m, 1H, ar); 7.40–7.49 (m, 3H, ar); 7.66–7.77 (m, 2H, ar) ppm. ¹³C-NMR (MeOD, δ): 10.55 (CH₃), 18.10 (CH₂), 24.25 (CH₂), 31.34 (CH₂), 45.25 (CH₂), 78.77 (C), 91.84 (C), 123.75 (C), 123.96 (CH), 128.01 (CH), 129.12 (CH), 129.15 (C), 130.69 (CH), 133.21 (C), 134.37 (CH), 134.65 (CH), 138.85 (C), 151.46 (C), 154.99 (C), 170.27 (C),

170.78 (C) ppm. HRMS (m/z) calculated for [M + H]⁺ ion species C₂₃H₂₂N₅O₂: 400.1768; found 400.1765.

Methyl (S)-2-(2-oxo-5-phenyl-2,3-dihydro-1H-benzo[e][1,4]diazepin-3-yl)acetate 13

2-Amino-benzophenone (0.096 g, 0.5 mmol) and methyl (S)-3-(((9H-fluoren-9-yl)methoxy)carbonyl)amino)-4-chloro-4-oxo-butanoate [33] (1 eq) were mixed in CHCl₃ and heated under reflux for 3 h. After disappearance of the starting material (TLC, CH₂Cl₂/MeOH 99:1), the residue was partitioned between CH₂Cl₂ and NaHCO₃ (saturated solution). Drying (Na₂SO₄) and removal of solvent gave **12**, which was used as such in the following step: it was dissolved in THF, treated with an excess of piperidine (12 eq) and left stirring at room T for 1 h. Glacial acetic acid (20 eq) was added, and the mixture was left stirring at room T for 2 h. The solvent was removed and the residue partitioned between CH₂Cl₂ and H₂O; the organic layer was washed with NaHCO₃ (saturated solution). Drying (Na₂SO₄) and removal of solvent gave a residue which was purified by flash chromatography (hexane/ethyl acetate 1:1), obtaining the title compound in 83% yield. ¹H-NMR (CDCl₃, δ): 3.22 (dd, J = 16.8, 6.4 Hz, 1H); 3.47 (dd, J = 16.8, 7.6 Hz, 1H); 3.75 (s, 3H); 4.16 (t, J = 6.8 Hz, 1H); 7.10–7.16 (m, 1H); 7.19–7.22 (m, 1H); 7.30–7.37 (m, 3H); 7.38–7.42 (m, 1H); 7.45–7.52 (m, 3H); 8.43 (s, 1H, NH) ppm. ¹³C-NMR (CDCl₃, δ): 36.44 (CH₂), 51.70 (CH), 60.26 (CH₃), 121.41 (CH), 123.42 (CH), 127.45 (C), 128.16 (CH), 129.84 (CH), 130.35 (CH), 131.25 (CH), 131.82 (CH), 138.37 (C), 139.08 (C), 169.87 (C), 171.51 (C), 172.41 (C) ppm.

Methyl (S)-2-(5-phenyl-2-thioxo-2,3-dihydro-1H-benzo[e][1,4]diazepin-3-yl)acetate 14

Phosphorus pentasulfide (0.183 g, 0.4 mmol) and Na₂CO₃ (0.044 g, 0.4 mmol) were mixed with 1,2-dichloroethane (3 mL) and stirred at room T for 2 h, then **13** (0.07 g, 0.23 mmol) was added and the mixture heated at 65 °C for 4 h. After cooling the solvent was removed and the residue purified by flash chromatography (hexane/ethyl acetate 1:1), obtaining methyl (S)-2-(5-phenyl-2-thioxo-2,3-dihydro-1H-benzo[e][1,4]diazepin-3-yl)acetate **14** in 50% yield. ¹H-NMR (CDCl₃, δ): 3.45 (dd, J = 16.8, 6.8 Hz, 1H); 3.65 (dd, J = 16.8, 6.8 Hz, 1H); 3.72 (s, 3H); 4.37 (t, J = 6.8 Hz, 1H); 7.17–7.23 (m, 2H); 7.29–7.33 (m, 3H); 7.39–7.41 (m, 1H); 7.44–7.52 (m, 3H); 10.55 (s, 1H, NH) ppm.

Methyl (S)-2-(1-methyl-6-phenyl-4H-benzof[1,2,4]triazolo[4,3-a][1,4]diazepin-4-yl)acetate 16

Compound **14** was treated with hydrazine (2 eq) in THF maintaining the temperature below 15 °C. When the starting material was consumed (TLC, CH₂Cl₂/MeOH/NH₃ 93:7:03),

the solvent was removed and the residue treated with H₂O and extracted with CH₂Cl₂. Drying (Na₂SO₄) and removal of solvent gave a residue (**15**) which was used as such for the following step: it was dissolved in THF (5 mL), the temperature was cooled to 0 °C and acetyl chloride (1.05 eq) and diisopropyl-ethylamine (1q) were added. After 1 h stirring at low temperature, the solvent was removed under vacuum, the residue was treated with glacial acetic acid and heated under reflux for 0.5 h. Removal of the solvent gave a residue which was purified by flash chromatography (CH₂Cl₂/MeOH/NH₃ 9:1:0.1) obtaining the title compound in 53% yield. ¹H-NMR (CDCl₃, δ): 2.59 (s, 3H, CH₃); 3.59 (d, J = 7.2 Hz, 2H, CH₂); 3.71 (s, 3H, OCH₃); 4.56 (t, J = 7.2 Hz, 1H, CH); 7.28–7.32 (m, 2H, ar); 7.36–7.48 (m, 6H, ar); 7.51–7.57 (m, 1H, ar) ppm. ¹³C-NMR (CDCl₃, δ): 12.22 (CH₃), 36.77 (CH₂), 51.85 (CH), 53.12 (OCH₃), 123.41 (CH), 127.37 (CH), 128.21 (CH), 129.00 (CH), 129.30 (C), 129.48 (CH), 130.64 (CH), 131.64 (CH), 132.02 (CH), 133.41 (C), 138.85 (C), 150.60 (C), 156.42 (C), 167.74 (C), 172.08 (C) ppm.

(S)-2-(1-Methyl-6-phenyl-4H-benzo[f][1,2,4]triazolo[4,3-a][1,4]diazepin-4-yl)acetic acid 17

Compound **16** (0.141 g, 0.48 mmol) was dissolved in 1:1 MeOH/THF (5 mL), NaOH (2 mL of a 1 M solution) was added, and the mixture was left stirring at room T for 2 h. After consumption of the starting material (TLC, CH₂Cl₂/MeOH 93:7) 1 M HCl was added dropwise until a white precipitate was formed, which was filtered and dried. The title compound was obtained in 81% yield. ¹H-NMR (CDCl₃, δ): 2.70 (s, 3H, CH₃); 3.60 (dd, J = 16 Hz, 6.8 Hz, 1H, CHH); 3.69 (dd, J = 16 Hz, 7.2 Hz, 1H, CHH); 4.56 (t, J = 6.8 Hz, 1H, CH); 7.23–7.33 (m, 2H, aromatic); 7.34–7.46 (m, 6H, aromatic); 7.63–7.69 (m, 1H, aromatic) ppm. ¹³C-NMR (MeOD, δ): 10.41 (CH); 35.81 (CH₂); 52.83 (CH); 123.82 (CH), 127.73 (CH), 127.92 (CH), 128.20 (CH), 128.40 (CH), 129.20 (C), 129.32 (CH), 130.54 (CH), 131.62 (CH), 132.01 (CH), 133.03 (C), 138.79 (C), 156.61 (C), 168.94 (C), 173.09 (C).

Methyl (S)-7-(2-(1-methyl-6-phenyl-4H-benzo[f][1,2,4]triazolo[4,3-a][1,4]diazepin-4-yl)acetamido)heptanoate 18

Compound **17** (0.11 g, 0.33 mmol), methyl 7-aminoheptanoate (0.063 g, 0.39 mmol), HATU (0.15 g, 0.39 mmol) and Et₃N (0.092 mL, 0.66 mmol) were dissolved in DMF (5 mL) and left stirring at room T overnight. After removal of the solvent under vacuum, the residue was partitioned between brine and ethyl acetate; the organic layer was collected and dried (Na₂SO₄), then the solvent was removed under vacuum and the residue purified by flash chromatography (abs EtOH/CH₂Cl₂/pet. ether/NH₃ 65:340:60:8 as eluent) obtaining the title compound in 76% yield. ¹H-NMR (CDCl₃, δ): 1.21–1.28 (m, 4H); 1.45–1.61 (m, 4H); 2.22 (t, J = 7.6 Hz, 2H, CH₂CO); 2.59 (s, 3H, CH₃);

3.14–3.28 (m, 2H, CH₂N); 3.31 (dd, J = 14.0, 6.8 Hz, 1H, CHH); 3.48 (dd, J = 14.0, 6.8 Hz, 1H, CHH); 3.62 (s, 3H, OCH₃); 4.56 (t, J = 6.8 Hz, 1H, CH); 6.70 (t, J = 5.6 Hz, 1H, NH); 7.27–7.30 (m, 2H, aromatics); 7.35–7.45 (m, 6H, aromatics); 7.58–7.64 (m, 1H, aromatic) ppm. ¹³C-NMR (CDCl₃, δ): 12.16 (CH₃), 24.79 (CH₂), 26.51 (CH₂), 28.72 (CH₂), 29.29 (CH₂), 33.94 (CH₂), 39.30 (CH₂), 39.48 (CH₂), 51.43 (CH), 53.83 (OCH₃), 123.45 (CH), 127.40 (CH), 128.19 (CH), 129.32 (C), 129.46 (CH), 131.43 (CH), 131.61 (CH), 131.99 (CH), 133.28 (C), 138.83 (C), 150.52 (C), 156.38 (C), 167.74 (C), 170.54 (C), 174.17 (C) ppm. ESI-MS m/z (C₂₇H₃₁N₅O₃) 474.1 [M + H]⁺, 496.1 [M + Na]⁺.

((S)-N-hydroxy-7-(2-(1-methyl-6-phenyl-4H-benzo[f][1,2,4]triazolo[4,3-a][1,4]diazepin-4-yl)acetamido)heptanamide 6 (SUM52)

A solution of KOH (0.7 g, 12.5 mmol) in MeOH (2 mL) was added dropwise to a solution of hydroxylamine hydrochloride (0.58 g, 8.4 mmol) in MeOH (3 mL) at 0 °C. After stirring at the same T for 0.5 h, the solution was filtered, compound **18** (0.119 g, 0.25 mmol) was added and the mixture was left stirring at room T for 1 h. The solvent was removed under vacuum and the residue was purified by flash chromatography (CH₂Cl₂/MeOH 9:1). A fraction was collected, consisting in a mixture of the desired product and of the carboxylic acid analogue; this mixture was partitioned between sat. NaHCO₃ and ethyl acetate, the organic layer was collected, dried (Na₂SO₄), the solvent was removed under vacuum affording the title compound as a white solid in 25% yield. M. p. 169–172 °C. ¹H-NMR (CDCl₃, δ): 1.20–1.70 (m, 8H); 2.14–2.20 (m, 2H, CH₂CO-hydroxamate); 2.65 (s, 3H, CH₃); 3.03–3.12 (m, 1H, NCHH); 3.28–3.47 (m, 2H, CHHCONCHH); 3.59–3.72 (m, 1H, CHHCO); 4.70–4.74 (m, 1H, CH); 7.30–7.78 (m, 9H, aromatic) ppm. ¹³C-NMR (CDCl₃, δ): 12.07 (CH₃), 24.67 (CH₂), 27.79 (CH₂), 28.70 (CH₂), 29.69 (CH₂), 32.02 (CH₂), 38.90 (CH₂), 53.79 (CH), 123.69 (CH), 127.69 (CH), 128.75 (CH), 129.38 (C), 129.55 (CH), 130.79 (CH), 131.72 (CH), 132.04 (CH), 133.01 (C), 138.71 (C), 150.81 (C), 156.82 (C), 168.07 (C), 170.45 (C), 171.23 (C) ppm. HRMS (m/z) calculated for [M + H]⁺ ion species C₂₆H₃₁N₆O₃: 475.2452; found 475.2450.

FRET bromodomain binding assay

The reader assay is a binding assay using AlphaScreen technology FRET assay, and was performed by Reaction Biology (www.reactionbiology.com). The biotinylated peptide binding to the reader domain of His-tagged protein is monitored by the singlet oxygen transfer from the Streptavidin-coated donor beads to the AlphaScreen Ni-chelate acceptor beads. The reagents, proteins and the applied experimental protocol is reported below as provided by Reaction Biology.

Reagent

Reaction buffer: 50 mM Hepes, pH7.5, 100 mM NaCl, 0.05% CHAPS, 0.1% BSA, and 1% DMSO (the final DMSO concentration may differ depending on compound stock and test concentrations).

Bromodomain

BRD4-1: RBC Cat# RD-11-140: Recombinant Human Bromodomain containing protein 4, bromodomain 1 (aa 44-170; Genbank Accession # NM_058243), expressed in *E. coli* with N-terminal His-tag. MW = 17.8 kDa.

BRD4-2: RBC Cat# RD-11-141: Recombinant Human Bromodomain containing protein 4, bromodomain 2 (aa 349-460; Genbank Accession # NM_058243), expressed in *E. coli* with N-terminal His-tag. MW = 15.7 kDa.

Ligand (C-term-Biotin)

Histone H4 peptide (1–21) K5/8/12/16Ac-Biotin.

Detection beads: PerkinElmer

Donor beads: Streptavidin-coated donor beads; Acceptor beads: AlphaScreen Ni acceptor beads.

Reaction procedure

1. Deliver 2.5X BRD in wells of reaction plate except No BRD control wells. Add buffer instead.
2. Deliver compounds in 100% DMSO into the BRD mixture by Acoustic technology (Echo550; nanoliter range). Spin down and pre-incubation for 30 min.
3. Deliver 5X Ligand. Spin and shake.
4. Incubate for 30 min at room temperature with gentle shaking.
5. Deliver 5X donor beads. Spin and shake.
6. Deliver 5X acceptor beads. Spin and shake. Then gentle shaking in the dark for 60 min.
7. Alpha measurement (Ex/Em = 680/520–620 nm) in Enspire.

HDACs inhibition assay

HDAC assay

To test the inhibition activity of all compounds, we used the HDAC1 Immunoprecipitation (IP) & Activity Assay Kit (Catalog # K342-25; Biovision). To perform the experiment, we used the protocol provided by the kit.

HCT-116 cell lines were plated in 6 wells and treated with the compounds **5** and **6** at 10 μ M for 12 h. After incubation the media was removed and the cells were washed with PBS (EuroClone) solution (2X). Then, 200 μ l/well of Lysis Buffer with protease inhibitor was added and the cells were scraped and incubated in ice for 30 min. After centrifugation at 10,000 \times g for 10 min at 4 $^{\circ}$ C, the supernatant was collected. 100 μ g of each extract were incubated with 6 μ l of Rabbit HDAC1 Antibody and Rabbit IgG and the volume was reached to 500 μ l with PBS with protease inhibitors. After incubation at 4 $^{\circ}$ C overnight a rotary mixer, 25 μ l of the protein-A/G bead slurry, previously washed with PBS (2X), was added to the samples and incubated for 1 h at 4 $^{\circ}$ C. The beads were recovered after 3 washed with 1 ml PBS, by centrifuging at 14,000 \times g for ~10 s and used for HDAC assay.

HDAC assay preparation

For each reaction, 168 μ l Reaction Mix containing HDAC Assay Buffer and HDAC Substrate was prepared, added to the sample and to background control tube, and incubated at 37 $^{\circ}$ C for 2 h. SAHA was used as a positive control. To measure the total HDAC activity, 3 μ l of Positive control was incubated with 4 μ l HDAC Substrate in a final volume of 180 μ l with HDAC Assay Buffer. Then, 20 μ l of the Developer were added and incubated for 30 min at 37 $^{\circ}$ C. The samples were centrifuged and 100 μ l transferred in a black flat plate. The fluorescence was read at Ex/Em = 380/500 nm with Tecan M1000 plate reader.

Cell lines

HCT-116, colon cancer cells were propagated in Dulbecco's Modified Eagle's Medium (Euroclone, Milan, Italy) with 10% fetal bovine serum (FBS; Euroclone), 2 mM L-glutamine (Euroclone), and antibiotics (100 U/ml penicillin, 100 mg/ml streptomycin; Euroclone).

Total protein extraction

HCT-116 cells were treated with the molecules for 24 h at 5 μ M. Tubastatin A (Tub.A) was used as positive control at 10 μ M. Then, the cells were harvested, washed with PBS (2X) (Euroclone) and lysed in protein extraction buffer containing H₂O with 50 mM Tris HCl pH 8.0 solution, 5 mM EDTA, 1% NP40, 150 mM NaCl, 0.5% sodium deoxycholate, 0.1% SDS, and 1X protein inhibitor protease. After incubation, for 15 min at 4 $^{\circ}$ C, the samples were centrifuged at 13,000 rpm at 4 $^{\circ}$ C for 30 min, and the supernatant was recovered. 40 μ g of total protein, determined by a Bradford assay (Bio-Rad, Milan, Italy), were

used for the Western blot. Antibodies used were: ac-Tubulin (T5168; Sigma) and GAPDH (sc-47724; Santa Cruz Biotechnology).

Antitumor activity

Dulbecco's Modified Eagle's Medium (DMEM), Nutrient Mixture F-12 Ham, fetal calf serum (FCS), penicillin/streptomycin and *L-Glutamine* were purchased from Sigma-Aldrich (Milan, Italy); C26 murine colon carcinoma cells and human neuroblastoma SH-SY5Y cells were obtained from American Type Culture Collection (ATCC, Manassa, VA, USA). High capacity cDNA-Reverse Transcription kit and Syber Green Master Mix were from Life Technologies (Eugene, OR, USA).

Tali Cell Cycle Kit was from Life Technologies (Eugene, OR, USA).

Cell culture and treatments

C26 colon carcinoma cells were cultured in high-glucose DMEM supplemented with 1% *L*-glutamine, 1% penicillin/streptomycin and 10% fetal bovine serum (FBS) (growth medium) and maintained in a humidified atmosphere containing 5% CO₂ at 37 °C, as suggested by the company [36].

SSM2C melanoma cells were isolated from two skin metastases that were excised from the same individual 1 and 4 months after diagnosis, respectively. After dissociation and filtration, cells were grown in high-glucose DMEM with 10% FBS supplemented with 1% *L*-glutamine, 1% penicillin/streptomycin as reported [37].

Human neuroblastoma SH-SY5Y cells were grown in DMEM/HAM's F-12 supplemented with 10% heat-inactivated FBS, 1% *L*-glutamine and 100 U/mL penicillin/streptomycin as described in ref. [38]. The cells were maintained at 37 °C in a humidified incubator with 5% CO₂ and 95% air.

Cell medium was changed every other day and the cells were split (0.25% trypsin, 0.53 mM EDTA solution) when they reached ~80% confluence. All treatments were performed using cells at ~60–70% confluence.

For cell proliferation analysis by cell counting and for cytometry analysis of the cell cycle distribution, cells were incubated for the indicated time and concentration with compound **5**, compound **6** or IBET762.

Cell proliferation was determined by cell counting using Burker camera. Specifically, cells were plated at a density of 15×10^4 cells/well in a 6-well plate in growth medium, synchronized and treated as reported above. Cytometric analysis was performed using The Tali[®] Image-Based Cytometer (Thermo Fisher Scientific), a 3-channel benchtop assay platform that captures up to 20 images (fields of view) per sample, automatically analyses the images with

sophisticated digital image-based cell counting and fluorescence detection algorithms [39]. The Tali[®] Cell Cycle Kit was used to count living and dead cells and the percentage of cells in each phase of the cell cycle. Aliquot of cells ($0.5\text{--}1 \times 10^6$) from each sample were collected and fixed with ice-cold 70% ethanol in to a concentration of 1×10^6 to -5×10^6 cells/mL. The samples were placed at least for a night at -20 °C, then ethanol was removed and cells were stained with propidium iodide incubating them at room temperature for 30 min in the dark with the Tali[®] Cell Cycle Solution. Cell suspension (25 μ L) was transferred in the dedicated slide and cell cycle analysis was performed using the Tali[®] Image-Based Cytometer (Thermo Fisher Scientific, Carlsbad, CA, USA). The percentage of cells in each phase of the cell cycle was determined using FCS Express Research Edition software (version 4.03; De Novo Software, Morristown, NJ, USA).

Preparation of RNA and measurement of gene expression by quantitative real-time polymerase chain reaction

p21 mRNA levels were quantified by real-time PCR in human neuroblastoma SHSY5Y cells. Specific primers for P21 and the housekeeping Glyceraldehyde-3-Phosphate Dehydrogenase gene (GAPDH) were designed using the program NCBI BLAST NUCLEOTIDE (Rockville Pike, Bethesda, MD, USA). GAPDH mRNA represents the endogenous control useful for the normalization of mRNA concentrations. Total RNA was prepared using TRIzol reagent (Thermo Fisher Scientific, Carlsbad, CA, USA). Quantity and quality of the RNA extracts were quantified using a Nanodrop (Thermo Scientific, Carlsbad, CA, USA). First strand cDNA was synthesized in reverse transcription reaction (20 μ L) with 0.5 μ g RNA by using the high capacity cDNA-Reverse-Transcription kit (Life Technologies, Carlsbad, CA, USA). The reaction conditions were kept for 10 min at 25 °C, 120 min at 37 °C, 5 min at 85 °C. The Real-Time PCR reaction was performed as described [40] using cDNA 100 ng, 0.25 μ M of each primer (Primers stocks 100 μ M, Sigma-Aldrich, Milan, Italy) and Power SYBR Green PCR Master Mix (Life Technologies, Carlsbad, CA, USA). The gene amplification was conducted in an MIC (Diatech Pharmacogenetics, Jesi, AN, Italy): 95 °C for 10 min, followed by 40 cycles at 95 °C for 30 s, 58 °C for 30 s, 72 °C for 45 s, 95 °C for 15 s, 60 °C for 60 s, 95 °C for 15 s and 60 °C for 15 s. The sequences of the primers are here listed: GAPDH forward: 5'-GGCAAATTCAACGGC ACAGTC-3', GAPDH reverse: 5'-TCGCTCCTGGAAG ATGGTG-3'; P21 forward: 5'-CTG GTG GCA GTG CTG ACT G-3', P21 reverse: 5'-GCT CTG CTC AGG GGA CAT AC-3'. Both positive and negative controls were included in the analysis. Relative P21 transcript levels were calculated: fold = $2^{-\Delta\Delta C_t}$ as reported [40] (ΔC_t , difference in

Ct between the target gene and the housekeeping one; $\Delta\Delta C_t$, difference between the ΔC_t of the interest sample and the ΔC_t of the reference one). mRNA levels in vehicle were arbitrarily set to 100.

Presentation of data and statistical analysis

Results are expressed as mean \pm SEM of at least three independent experiments. Statistical significance was determined by two-sided Student's *t* test, with a value of $p < 0.05$ considered significant. In multiple comparisons, statistical significance was determined using ANOVA and Newman–Keuls post-test, Pearson Index. Calculations were performed using GraphPad INSTAT + 3.3 software (GraphPad, San Diego, CA, USA).

Antihyperalgesic activity

Animals and ethics approval

Male CD1 mice (24–26 g, 4 weeks old) from the Harlan Laboratories (Bresso, Italy) were used. Mice were randomly assigned to standard cages, with 4 to 5 animals per cage. The cages were placed in the experimental room 24 h before behavioral test for acclimatization. The animals were fed a standard laboratory diet and tap water ad libitum and kept at 23 \pm 1 °C with a 12 h light/dark cycle, light on at 7 a.m. Experiments were carried out in accordance with international laws and policies (Directive 2010/63/EU of the European parliament and of the council of 22 September 2010 on the protection of animals used for scientific purposes; Guide for the Care and Use of Laboratory Animals, US National Research Council, 2011). Protocols were approved by the Animal Care and Research Ethics Committee of the University of Florence, Italy, under license from the Italian Department of Health (410/2017-PR).

Animal studies are reported in compliance with the animal research: reporting of in vivo experiments (ARRIVE) guidelines [41]. Protocols were designed to minimize the number of animals used and their suffering.

Mice were sacrificed by cervical dislocation for removal of spinal cord for in vitro analyses. The number of animals per experiment was based on a power analysis and calculated by G power software. To determine behavioral parameters, each tested group comprised 8 animals.

Intranasal (i.n.) administration

For i.n. administration, mice were slightly anesthetized by 2% isoflurane inhalation and placed in a supine position [42]. A 5 μ l aliquots of solution (treatments or vehicle) was slowly dropped alternatively to each nostril with a micropipette tip.

Spared nerve injury (SNI)

Behavioral testing was performed before surgery to establish a baseline for comparison with postsurgical values. Mono-neuropathy was induced as previously described [34]. Briefly, mice anesthetized with a mixture of 4% isoflurane in O₂/N₂O (30:70 v/v) and placed in a prone position. The right hind limb was immobilized in a lateral position and slightly elevated. Incision was made at mid-thigh level using the femur as a landmark. The sciatic nerve was exposed at mid-thigh level distal to the trifurcation and freed of connective tissue; the three peripheral branches (sural, common peroneal, and tibial nerves) of the sciatic nerve were exposed without stretching nerve structures. Both tibial and common peroneal nerves were ligated and transected together. A microsurgical forceps with curved tips was delicately placed below the tibial and common peroneal nerves to slide the thread (5.0 silk, Ethicon; Johnson & Johnson Intl, Brussels, Belgium) around the nerves. A tight ligation of both nerves was performed. The sural nerve was carefully preserved by avoiding any nerve stretch or nerve contact with surgical tools. Muscle and skin were closed in two distinct layers with silk 5.0 suture. Intense, reproducible, and long-lasting thermal hyperalgesia and mechanical allodynia-like behaviors are measurable in the non-injured sural nerve skin territory. The SNI model offers the advantage of a distinct anatomical distribution with an absence of co-mingling of injured and non-injured nerve fibers distal to the lesion such as the injured and not injured nerves, and territories can be readily identified and manipulated for further analysis (i.e., behavioral assessment). The sham procedure consisted of the same surgery without ligation and transection of the nerves.

Nociceptive behavior

Animals were habituated to the testing environment daily for at least 2 days before baseline testing. To evaluate onset and progression of pain hypersensitivity, neuropathic mice were monitored by measuring nociceptive responses every 30 min for 3 h before surgery or 3, 7, 10, and 14 days after nerve surgery. Experiments were performed on post-surgery day 14 when the pain hypersensitivity was well established. Each mouse served as its own control, the responses being measured both before and after surgery. All testing was performed with a blind procedure.

Mechanical allodynia

Mechanical allodynia was measured using Dynamic Plantar Anesthesiometer (Ugo Basile, Bologna, Italy), as previously described [43]. The mice were placed in individual Plexiglas cubicles (8.5 cm L, 3.4 cm H, and 3.4 cm B) on a wire mesh platform and allowed to acclimate for ~1 h, during which

exploratory and grooming activity ended. After that, the mechanical stimulus was delivered to the plantar surface of the hind paw of the mouse from below the floor of the test chamber by an automated testing device. A steel rod (2 mm) was pushed with electronic ascending force (0–5 g in 35 s). When the animal withdrew its hind paw, the mechanical stimulus was automatically withdrawn, and the force recorded to the nearest 0.1 g. Nociceptive response for mechanical sensitivity was expressed as mechanical paw withdrawal threshold in grams. Paw withdrawal threshold was quantified by an observer masked to the treatment. The mean paw withdrawal threshold was calculated from 6 consecutive trials (each performed every 30 min) and averaged for each group of mice.

Hargreaves' plantar test

Thermal nociceptive threshold was measured using Hargreaves' device and performed as previously described [44]. Paw withdrawal latency in response to radiant heat (infrared) was assessed using the plantar test apparatus (Ugo Basile, Comerio, Italy). Each mouse was placed under a transparent Plexiglas box (7.0312.5 cm², 17.0 cm high) on a 0.6 cm thick glass plate and allowed to acclimatize for 1 to 2 h before recording. The radiant heat source consisted of an infrared bulb (Osram halogen-bellaphot bulb, 8 V, 50 W; Osram, Italy) that was positioned 0.5 cm under the glass plate directly beneath the hind paw. The time elapsed between switching on the infrared radiant heat stimulus and manifestation of the paw withdrawal response was measured automatically. The intensity of the infrared light beam was chosen to give baseline latencies of 10 sec in control mice. A cutoff of 20 s was used to prevent tissue damage. Each hind paw was tested 2 to 3 times, alternating between paws with an interval of at least 1 min between tests. The interval between 2 trials on the same paw was of at least 5 min. Nociceptive response for thermal sensitivity was expressed as thermal paw withdrawal latency in sec. All determinations were averaged for each animal.

Acknowledgements This work was supported by: A.I.L. for fellowship and Fondazione Cassa di Risparmio di Firenze (2018.0998); V: ALERE; Campania Regional Government Technology Platform "Lotta alle Patologie Oncologiche": iCURE; Campania Regional Government FASE2: IDEAL; MIUR, Proof of Concept POC01_00043.

Compliance with ethical standards

Conflict of interest The authors declare no competing interests.

Publisher's note Springer Nature remains neutral with regard to jurisdictional claims in published maps and institutional affiliations.

Open Access This article is licensed under a Creative Commons Attribution 4.0 International License, which permits use, sharing,

adaptation, distribution and reproduction in any medium or format, as long as you give appropriate credit to the original author(s) and the source, provide a link to the Creative Commons license, and indicate if changes were made. The images or other third party material in this article are included in the article's Creative Commons license, unless indicated otherwise in a credit line to the material. If material is not included in the article's Creative Commons license and your intended use is not permitted by statutory regulation or exceeds the permitted use, you will need to obtain permission directly from the copyright holder. To view a copy of this license, visit <http://creativecommons.org/licenses/by/4.0/>.

References

- Allis CD, Jenuwein T. The molecular hallmarks of epigenetic control. *Nat Rev Genet.* 2016;17:487–500. <https://doi.org/10.1038/nrg.2016.59>.
- Falkenberg KJ, Johnstone RW. Histone deacetylases and their inhibitors in cancer, neurological diseases and immune disorders. *Nat Rev Drug Discov.* 2014;13:673–91. <https://doi.org/10.1038/nrd4360>.
- Tomaselli D, Lucidi A, Rotili D, Mai A. Epigenetic polypharmacology: a new frontier for epi-drug discovery. *Med Res Rev.* 2020;40:190–244. <https://doi.org/10.1002/med.21600>.
- Roche J, Bertrand P. Inside HDACs with more selective HDAC inhibitors. *Eur J Med Chem.* 2016;121:451–83. <https://doi.org/10.1016/j.ejmech.2016.05.047>.
- Zhang G, Smith SG, Zhou M-M. Discovery of chemical inhibitors of human bromodomains. *Chem Rev.* 2015;115:11625–68. <https://doi.org/10.1021/acs.chemrev.5b00205>.
- Lu T, Lu W, Luo C. A patent review of BRD4 inhibitors (2013–2019). *Expert Opin Ther Pat.* 2020;30:57–81. <https://doi.org/10.1080/13543776.2020.1702645>.
- Ramadoss M, Mahadevan V. Targeting the cancer epigenome: synergistic therapy with bromodomain inhibitors. *Drug Discov Today.* 2018;23:76–89. <https://doi.org/10.1016/j.drudis.2017.09.011>.
- de Lera AR, Ganesan A. Epigenetic polypharmacology: from combination therapy to multitargeted drugs. *Clin Epigenet.* 2016;8:105. <https://doi.org/10.1186/s13148-016-0271-9>.
- Romanelli MN, Borgonetti V, Galeotti N. Dual BET/HDAC inhibition to relieve neuropathic pain: Recent advances, perspectives, and future opportunities. *Pharmacol Res.* 2021;173:105901. <https://doi.org/10.1016/j.phrs.2021.105901>.
- Rodrigues DA, Pinheiro PdSM, Sagrillo FS, Bolognesi ML, Fraga CAM. Histone deacetylases as targets for the treatment of neurodegenerative disorders: Challenges and future opportunities. *Med Res Rev.* 2020;40:2177–211. <https://doi.org/10.1002/med.21701>.
- Kulikowski E, Rakai BD, Wong NCW. Inhibitors of bromodomain and extra-terminal proteins for treating multiple human diseases. *Med Res Rev.* 2021;41:223–45. <https://doi.org/10.1002/med.21730>.
- Lin S, Du L. The therapeutic potential of BRD4 in cardiovascular disease. *Hypertens Res.* 2020;43:1006–14. <https://doi.org/10.1038/s41440-020-0459-4>.
- Muller S, Filippakopoulos P, Knapp S. Bromodomains as therapeutic targets. *Expert Rev Mol Med.* 2011;13:e29. <https://doi.org/10.1017/S1462399411001992>.
- Descalzi G, Ikegami D, Ushijima T, Nestler EJ, Zachariou V, Narita M. Epigenetic mechanisms of chronic pain. *Trends Neurosci.* 2015;38:237–46. <https://doi.org/10.1016/j.tins.2015.02.001>.
- Wang W, Cui S-S, Lu R, Zhang H. Is there any therapeutic value for the use of histone deacetylase inhibitors for chronic pain? *Brain Res Bull.* 2016;125:44–52. <https://doi.org/10.1016/j.brainresbull.2016.04.010>.

16. Sánchez-Ventura J, Amo-Aparicio J, Navarro X, Penas C. BET protein inhibition regulates cytokine production and promotes neuroprotection after spinal cord injury. *J Neuroinflammation*. 2019;16:124. <https://doi.org/10.1186/s12974-019-1511-7>.
17. Takahashi K, Yi H, Liu C-H, Liu S, Kashiwagi Y, Patin DJ, et al. Spinal bromodomain-containing protein 4 contributes to neuropathic pain induced by HIV glycoprotein 120 with morphine in rats. *NeuroReport*. 2018;29:441–6. <https://doi.org/10.1097/wnr.0000000000000992>.
18. Zhang K, Xu Y. Suppressing BRD4 exhibits protective effects against vincristine-induced peripheral neuropathy by alleviating inflammation and oxidative stress. *Biochem Biophys Res Commun*. 2020;532:271–9. <https://doi.org/10.1016/j.bbrc.2020.06.142>.
19. Hsieh M-C, Ho Y-C, Lai C-Y, Wang H-H, Lee A-S, Cheng J-K, et al. Bromodomain-containing protein 4 activates voltage-gated sodium channel 1.7 transcription in dorsal root ganglia neurons to mediate thermal hyperalgesia in rats. *Anesthesiology*. 2017;127:862–77. <https://doi.org/10.1097/aln.0000000000001809>.
20. Borgonetti V, Galeotti N. Combined inhibition of histone deacetylases and BET family proteins as epigenetic therapy for nerve injury-induced neuropathic pain. *Pharmacol Res*. 2021;165:105431. <https://doi.org/10.1016/j.phrs.2021.105431>.
21. Cavaletti G, Marmiroli P. Chemotherapy-induced peripheral neurotoxicity. *Nat Rev Neurol*. 2010;6:657–66. <https://doi.org/10.1038/nrneurol.2010.160>.
22. Burgess J, Ferdousi M, Gosal D, Boon C, Matsumoto K, Marshall A, et al. Chemotherapy-induced peripheral neuropathy: epidemiology, pathomechanisms and treatment. *Oncol Ther*. 2021. <https://doi.org/10.1007/s40487-021-00168-y>.
23. Guandalini L, Cellai C, Laurenzana A, Scapocchi S, Paoletti F, Romanelli MN. Design, synthesis and preliminary biological evaluation of new hydroxamate histone deacetylase inhibitors as potential antileukemic agents. *Bioorg Med Chem Lett*. 2008;18:5071–4.
24. Cellai C, Balliu M, Laurenzana A, Guandalini L, Matucci R, Miniati D, et al. The new low-toxic histone deacetylase inhibitor S-(2) induces apoptosis in various acute myeloid leukemia cells. *J Cell Mol Med*. 2011;16:1758–65. <https://doi.org/10.1111/j.1582-4934.2011.01464.x>.
25. Laurenzana A, Balliu M, Cellai C, Romanelli MN, Paoletti F. Effectiveness of the histone deacetylase inhibitor (S)-2 against LNCaP and PC3 human prostate cancer cells. *PLOS ONE*. 2013;8:e58267. <https://doi.org/10.1371/journal.pone.0058267>.
26. Guandalini L, Balliu M, Cellai C, Martino MV, Nebbioso A, Mercurio C, et al. Design, synthesis and preliminary evaluation of a series of histone deacetylase inhibitors carrying a benzodiazepine ring. *Eur J Med Chem*. 2013;66:56–68. <https://doi.org/10.1016/j.ejmech.2013.05.017>.
27. Balliu M, Guandalini L, Romanelli MN, D'Amico M, Paoletti F. HDAC-inhibitor (S)-8 disrupts HDAC6-PP1 complex prompting A375 melanoma cell growth arrest and apoptosis. *J Cell Mol Med*. 2015;19:143–54. <https://doi.org/10.1111/jcmm.12345>.
28. Sanna MD, Guandalini L, Romanelli MN, Galeotti N. The new HDAC1 inhibitor LG325 ameliorates neuropathic pain in a mouse model. *Pharmacol Biochem Behav*. 2017;160:70–5. <https://doi.org/10.1016/j.pbb.2017.08.006>.
29. Filippakopoulos P, Picaud S, Fedorov O, Keller M, Wrobel M, Morgenstern O, et al. Benzodiazepines and benzotriazepines as protein interaction inhibitors targeting bromodomains of the BET family. *Bioorg Med Chem*. 2012;20:1878–86. <https://doi.org/10.1016/j.bmc.2011.10.080>.
30. Mirguet O, Gosmini R, Toum J, Clément CA, Barnathan M, Brusq J-M, et al. Discovery of epigenetic regulator I-BET762: lead optimization to afford a clinical candidate inhibitor of the BET bromodomains. *J Med Chem*. 2013;56:7501–15. <https://doi.org/10.1021/jm401088k>.
31. Filippakopoulos P, Qi J, Picaud S, Shen Y, Smith WB, Fedorov O, et al. Selective inhibition of BET bromodomains. *Nature*. 2010;468:1067–73. <https://doi.org/10.1038/nature09504>.
32. He S, Dong G, Li Y, Wu S, Wang W, Sheng C. Potent dual BET/HDAC inhibitors for efficient treatment of pancreatic cancer. *Angew Chem Int Ed*. 2020;59:3028–32. <https://doi.org/10.1002/anie.201915896>.
33. Kang CW, Ranatunga S, Sarnowski MP, Del Valle JR. Solid-Phase synthesis of tetrahydropyridazinedione-constrained peptides. *Org Lett*. 2014;16:5434–7. <https://doi.org/10.1021/o15026684>.
34. Borgonetti V, Governa P, Biagi M, Pellati F, Galeotti N. Zingiber officinale Roscoe rhizome extract alleviates neuropathic pain by inhibiting neuroinflammation in mice. *Phytomedicine*. 2020;78:153307. <https://doi.org/10.1016/j.phymed.2020.153307>.
35. Marshall AG, Hendrickson CL. High-resolution mass spectrometers. *Ann Rev Anal Chem*. 2008;1:579–99.
36. Ballarò R, Beltrà M, De Lucia S, Pin F, Ranjbar K, Hulmi JJ, et al. Moderate exercise in mice improves cancer plus chemotherapy-induced muscle wasting and mitochondrial alterations. *FASEB J*. 2019;33:5482–94. <https://doi.org/10.1096/fj.201801862R>.
37. Santini R, Vinci MC, Pandolfi S, Penachioni JY, Montagnani V, Olivito B, et al. HEDGEHOG-GLI signaling drives self-renewal and tumorigenicity of human melanoma-initiating cells. *Stem Cells*. 2012;30:1808–18. <https://doi.org/10.1002/stem.1160>.
38. Pierucci F, Garcia-Gil M, Frati A, Bini F, Martinesi M, Vannini E, et al. Vitamin D3 protects against A β peptide cytotoxicity in differentiated human neuroblastoma SH-SY5Y cells: a role for S1P1/p38MAPK/ATF4 axis. *Neuropharmacology*. 2017;116:328–42. <https://doi.org/10.1016/j.neuropharm.2017.01.003>.
39. Remple K, Stone L. Assessment of GFP expression and viability using the tali image-based cytometer. *JoVE*. 2011;57:e3659. <https://doi.org/10.3791/3659>.
40. Pierucci F, Frati A, Battistini C, Matteini F, Iachini MC, Vestri A, et al. Involvement of released sphingosine 1-phosphate/sphingosine 1-phosphate receptor axis in skeletal muscle atrophy. *Biochim Biophys Acta*. 2018;1864:3598–614. <https://doi.org/10.1016/j.bbadis.2018.08.040>.
41. McGrath JC, Lilley E. Implementing guidelines on reporting research using animals (ARRIVE etc.): new requirements for publication in *BJP*. *Br J Pharmacol*. 2015;172:3189–93. <https://doi.org/10.1111/bph.12955>.
42. Bortolozzi A, Castañé A, Semakova J, Santana N, Alvarado G, Cortés R, et al. Selective siRNA-mediated suppression of 5-HT1A autoreceptors evokes strong anti-depressant-like effects. *Mol Psychiatry*. 2012;17:612–23. <https://doi.org/10.1038/mp.2011.92>.
43. Sanna MD, Les F, Lopez V, Galeotti N. Lavender (*Lavandula angustifolia* Mill.) Essential oil alleviates neuropathic pain in mice with spared nerve injury. *Front Pharmacol*. 2019;10. <https://doi.org/10.3389/fphar.2019.00472>.
44. Sanna MD, Ghelardini C, Galeotti N. Activation of JNK pathway in spinal astrocytes contributes to acute ultra-low-dose morphine thermal hyperalgesia. *PAIN*. 2015;156:1265–75. <https://doi.org/10.1097/j.pain.000000000000164>.